https://doi.org/10.5194/wes-2026-225
Preprint. Discussion started: 25 November 2026
© Author(s) 2026. CC BY 4.0 License.



eawe european academy of wind energy
Open Access WIND ENERGY SCIENCE DISCUSSIONS

Atlas on leading-edge erosion risk in Europe based on IMERG

Charlotte Bay Hasager*, Abhiram Vinod, Laurids Dencker Di Stefano Toft, Krystallia Dimitriadou

Department of Wind and Energy Systems, Technical University of Denmark, Frederiksborgvej 399, 4000 Roskilde, Denmark;
abhvi@dtu.dk (A. V.); s224084@student.dtu.dk (L. D.D.S.T); krstd@dtu.dk (K. D.)

Correspondence to: Charlotte Bay Hasager (cbha@dtu.dk)

Abstract. Leading-edge erosion of wind turbine blades, triggered by precipitation, occurs across different climates in Europe. An atlas of spatial variability in erosion risk, both offshore and on land, is assessed using satellite-based rainfall observations from the GPM IMERG. GPM stands for the Global Precipitation Measurement satellite mission, and IMERG stands for Integrated Multi-satellitE Retrievals for GPM. Rainfall observations are combined with modelled wind speed from the New European Wind Atlas (NEWA), and the use of an empirical fatigue damage model derived from whirling-arm rain erosion test data from commercial coating. The 9-year series identify a positive Spearman correlation between wind and rainfall across most of Europe, particularly offshore, indicating that rainfall is more likely to occur in windy than in calm conditions in those regions. End of incubation varies from less than 4 years to more than 20 years, depending on location and turbine. Key results from the 5, 10, and 15 MW turbines are described. For the DTU 10 MW turbine, the end of incubation at the eight sites ranges from ~4 years (Buseco) to ~12 years (Rézentières). In regions at high risk of erosion, a potential solution to reduce damage is erosion-safe operation (ESO), i.e., slowing the blades during periods of high erosion. The atlas includes maps showing the extension of the end of incubation for expected annual energy production (AEP) loss for ESO at 0.2% and 0.4%, and maps showing expected AEP loss applying ESO to achieve a 5-, 10-, 15-, and 20-year end of incubation. Case-specific details on weather conditions, end of incubation, and ESO probabilistic Pareto fronts are presented for eight contrasting sites in Europe, including offshore, coastal, high-altitude flat, and complex terrains across Denmark, Finland, France, Italy, Spain, and the UK. The atlas is part of an effort to assess erosion risk relevant to planning wind farms, maintenance, and potentially applying erosion-safe operations. Main limitations are reduced IMERG quality for terrain with snowfall and very complex terrain.

1 Introduction

Rainfall does not noticeably damage wind turbine blades when the blades are at a standstill. When wind turbines produce electricity, the blade tip speeds are high, resulting in large relative velocities between the blades and impinging hydrometeors (Mishnaevsky et al., 2021; Pryor et al., 2025). Wind turbine blade leading-edge erosion (LEE) is primarily triggered by rainfall. The current study focuses on rainfall-driven LEE.

https://doi.org/10.5194/wes-2026-225
Preprint. Discussion started: 25 November 2026
© Author(s) 2026. CC BY 4.0 License.



eawe european academy of wind energy
Open Access WIND ENERGY SCIENCE DISCUSSIONS

In Europe, rainfall is the predominant hydrometeor. Snow is frequent at high altitudes and latitudes, while hail occurs mainly in convectively active regions such as the pre-Alpine areas (Punge and Kunz, 2016; Taszarek et al., 2020; Ghasemifard et al., 2024). In some regions of the US mainland, hail poses a significant risk to both solar plants and wind turbines (Pryor and Barthelmie, 2026), but hail is not considered in the current study, which covers Europe.

Spatial mapping of LEE at the national scale was initiated by Verma et al. (2021) using local precipitation and wind-speed observations from 31 sites across the Netherlands. It was subsequently extended by Nash et al. (2021) using local observations from 23 sites on the Island of Ireland, while results for Denmark covered 8 sites (Hasager et al., 2020). A comprehensive study covering the US mainland was based on local observations from 883 sites (Pryor et al., 2025). The length of the series varied from 16 to 30 years.

In contrast to the US, Europe lacks a harmonised, openly available continental database of co-located sub-hourly precipitation and wind-speed observations. Therefore, studies in Europe rely on alternatives.

One alternative is atmospheric numerical modeling. LEE was assessed from atmospheric modeling covering Northern Europe (Visbech et al., 2023), Scandinavia and surrounding seas (Hannesdóttir et al., 2024), and the Dutch North Sea and adjacent regions (Caboni and van Dalum, 2025). The time series covered 8, 5 and 10 years, respectively. An atlas on LEE covering Japan and the surrounding seas was based on 10 years of atmospheric numerical modeling (Sakai et al., 2026).

A second alternative is precipitation observations from satellites combined with numerically modeled wind speed. The global satellite-based precipitation product from IMERG, which stands for Integrated Multi-satellitE Retrievals for GPM, and GPM stands for the Global Precipitation Measurement satellite mission (Huffman et al., 2023), was used for assessment of LEE at various regions and sites in Europe (Badger et al., 2022; Dimitriadou et al., 2024, 2026; Visbech et al., 2025; Hasager et al., in review). The regions include the British Isles and surrounding seas, Navarra in Spain, and sites in Denmark, Germany, and Portugal. The time series varied from 5 to 10 years.

Several regional evaluations indicate that IMERG compares favourably with reanalysis and mesoscale-model precipitation in parts of Europe. Ivanova et al. (2025) reported that precipitation observations at three coastal sites in Belgium showed a higher correlation with IMERG than with the global reanalysis ERA5 (Hersbach et al., 2020) and the Norwegian reanalysis product NORA3 (Haakensstad et al., 2021; Solbrekke et al., 2021). Varga and Breuer (2024) showed IMERG correlates better with E-OBS than ERA5 and the Weather Research and Forecasting (WRF) mesoscale model (Skamarock et al., 2019). E-OBS is a gridded precipitation product based on local European observations (Cornes et al., 2018). E-OBS covers land areas only, not seas, and does not differentiate between liquid (rain) and solid precipitation (snow and hail). In contrast, the likelihood of liquid and solid hydrometeors can be estimated from their probabilistic contributions from IMERG (Xiong et al., 2022). Retalis et al. (2022) reported IMERG correlates better with E-OBS than other satellite-based products in the Mediterranean Region. Known weaknesses of IMERG include low-quality data for terrain with heavy snowfall and very complex terrain. Rain gauge calibration is performed over land, not offshore.

Erosion-safe operation (ESO) is a potential solution to reduce erosion with minimal loss of annual energy production (or income) by slowing the tip speed during severe rain events (Bech et al., 2018; Tilg et al., 2020; Castorrini et al., 2024). Research

https://doi.org/10.5194/wes-2026-225
Preprint. Discussion started: 25 November 2026
© Author(s) 2026. CC BY 4.0 License.



eawe european academy of wind energy
Open Access WIND ENERGY SCIENCE DISCUSSIONS

indicates potential benefits in delaying end of incubation and, to some extent, overall profit, e.g. in the US (Pryor et al., 2025) and the Netherlands (Caboni et al., 2024). An atlas on ESO is not available at the time of publication, to the authors' knowledge. The study fills the knowledge gap on the end of incubation and ESO efficiency at eight sites in Europe with contrasting climates, using a standardized dataset: rainfall from IMERG and wind speeds from NEWA. Furthermore, the study provides the first European atlas on end-of-incubation and erosion-safe operation efficiency.

The objectives of the current study include: i) to quantify the variability of erosion risk and potential of erosion-safe operation at eight sites relevant for wind energy and with highly variable weather conditions across Europe, ii) to produce a European atlas of leading-edge erosion risk using a standardized, long-term dataset. The atlas quantifies end-of-incubation and the efficiency of erosion-safe operation for three reference turbines.

2. Study area and meteorological data

2.1 Study area

The study area covers Europe from 34°N to 65°N latitude and 13°W to 32°E longitude. The climate zones range from cold to warm, from oceanic to continental.

Detailed analysis is presented for eight sites spanning Denmark, Finland, France, Italy, Spain, and the UK, including offshore, coastal, and high-altitude sites. Figure 1 shows the study area and indicates the location of the eight sites. The geographical coordinates of the sites are listed in Table 1.

https://doi.org/10.5194/wes-2026-225
Preprint. Discussion started: 25 November 2026
© Author(s) 2026. CC BY 4.0 License.

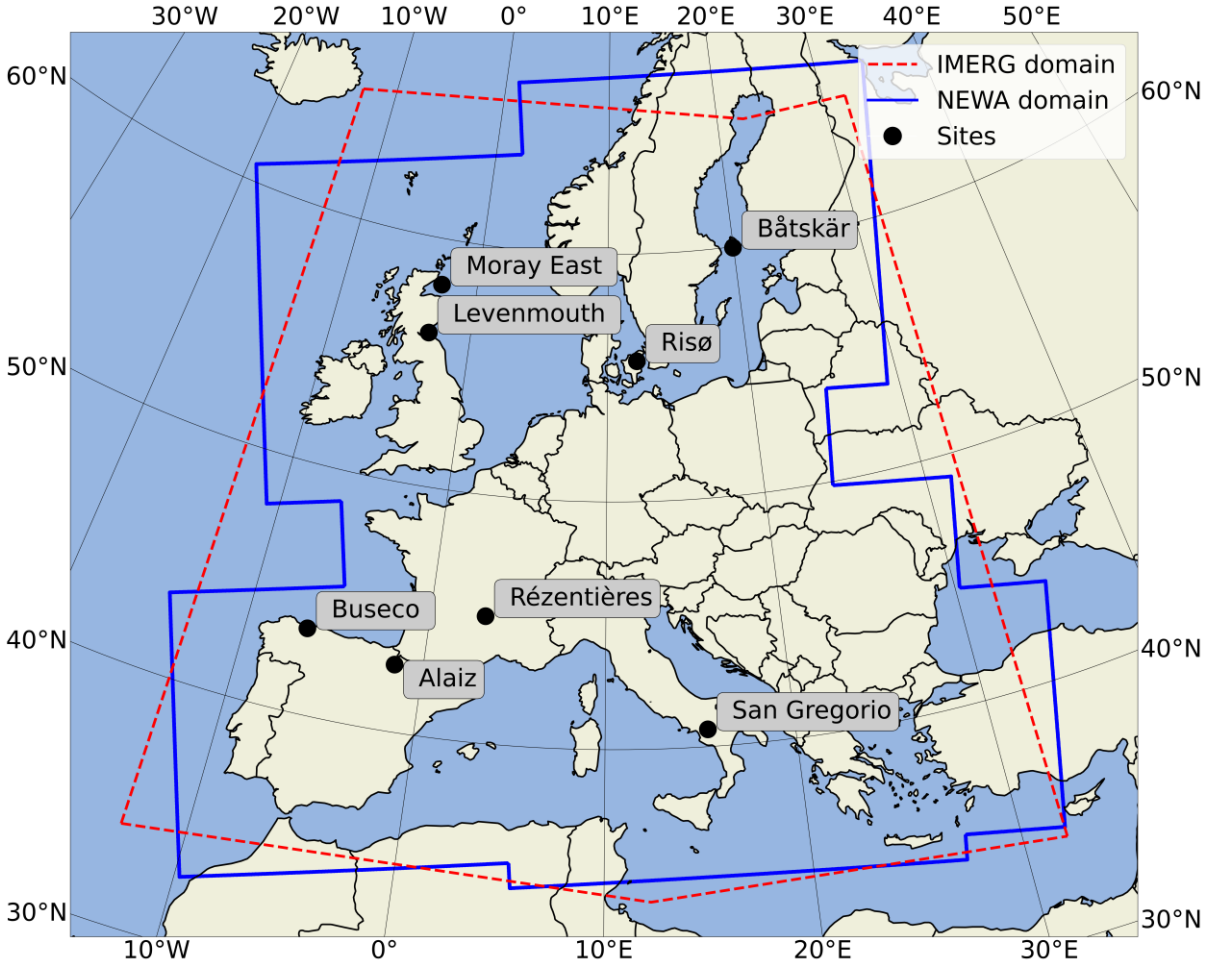


Figure 1: Study area and location of sites investigated. The domains of the extracted IMERG and NEWA data are visualized, and their intersection is utilized in the current study.

Table 1: Information about sites.

Site	Country	Latitude (° N)	Longitude (° E)	Height above sea level (m)	Type
Alaiz	ES	42.696	-1.555	1130	Complex
Båtskär	FI	59.963	19.956	0	Coastal
Buseco	ES	43.441	-6.643	917	Complex
Levenmouth	UK	56.174	-3.019	0	Offshore
Moray East	UK	58.167	-2.699	0	Offshore

https://doi.org/10.5194/wes-2026-225
Preprint. Discussion started: 25 November 2026
© Author(s) 2026. CC BY 4.0 License.

Rézentières	FR	45.112	3.120	1120	High-altitude flat
Risø	DK	55.694	12.088	0	Coastal
San Gregorio	IT	40.695	15.410	1125	Complex

2.2 Meteorological data

2.2.1 IMERG rainfall data

The IMERG dataset provides gridded, near-global precipitation estimates every 30 minutes with a spatial resolution of 0.1°. The IMERG Final Run precipitation product version 07 (IMERG-F V07B) corrected with monthly in situ gauge observations to reduce bias, was downloaded (Huffman et al., 2020, 2023). The IMERG-F V07B dataset precipitation, including *precipitationQualityIndex* and *probabilityLiquidPrecipitation* fields for the years 2014-2023, was extracted for the study area domain. IMERG data with *precipitationQualityIndex* below 0.4 were excluded to ensure sufficient data quality (Huffman et al., 2020). Fig. 2a shows a 30-minute precipitation event.

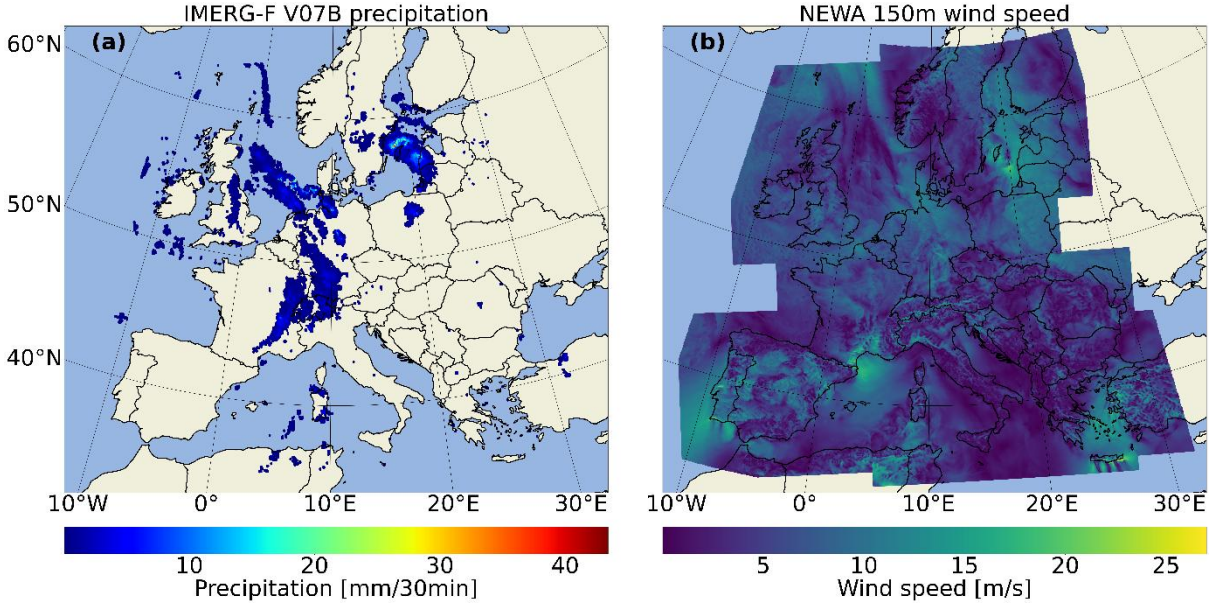


Figure 2: a) Precipitation event from IMERG-F V07B at 1 July 2022 01:00 UTC; b) Concurrent wind speed from NEWA at 150m altitude.

As the focus of this work is on rainfall's impact on wind turbine blades, solid precipitation types (e.g., snow, graupel, and hail) were removed from the dataset. Following the approach described in (Xiong et al., 2022), an empirical threshold of 50% for the IMERG *probabilityLiquidPrecipitation* parameter was applied to classify precipitation as liquid, thereby retaining only

https://doi.org/10.5194/wes-2026-225
Preprint. Discussion started: 25 November 2026
© Author(s) 2026. CC BY 4.0 License.



eawe european academy of wind energy
Open Access WIND ENERGY SCIENCE DISCUSSIONS

rainfall observations. IMERG V07 precipitation data are natively provided in units of mm h^{-1}; after quality control and filtering, the data were converted to half-hourly accumulated rainfall totals (mm per 30 min). The measurement resolution is 0.01 mm h^{-1}. IMERG at 11 km grid is re-gridded to 3 km to fit the spatial resolution of NEWA wind speeds. The NEWA in-built grid is the starting point for re-gridding. NEWA use an irregular grid while IMERG use a regular grid. The 2-dimensional interpolation is based on nearest neighbour to maintain original rain intensity values. IMERG provides only the rain intensity, and a calculation to droplet size and fall velocity of droplets are assumed to follow the function given by Best (1950).

2.2.2 NEWA wind speed data and vertical interpolation

NEWA model output covers Europe (Dörenkämper et al., 2020; NEWA, 2026). In our study, modelled wind speeds for the years 2014-2022 were extracted for the domain shown in Fig. 1. Modelled wind speeds at heights of 50, 75, 100, and 150 m were selected. NEWA wind speeds were extracted for one additional year (2023) for the eight sites listed in Table 1 but were not available in the entire domain. Therefore, the results for the domain (in Fig. 1) cover 9 years (2014-2022), while the results for the eight sites (Table 1) cover 10 years (2014-2023).

Wind speeds at heights between the NEWA-modelled wind-speed heights were calculated by vertical interpolation using the logarithmic wind profile as in Hasager et al. (in review). The interpolation was performed to 90 m and 119 m using the logarithmic for neutral stability conditions. These heights are the hub heights of the reference turbines: NREL 5MW (Jonkman et al., 2009) and DTU 10MW (Bak et al., 2013). Wind speeds at 150 m, the hub height of the reference turbine IEA 15 MW (Gaertner et al., 2020), were available from NEWA.

3. Methods

3.1 Weather statistics

The IMERG rainfall data and the NEWA wind speed data, both at 30-minute intervals, are collocated at the eight sites and in each grid cell across the entire domain using the nearest-neighbor approach and used to assess the Spearman correlation. Zero values are included, and for the resulting ties, the values are assigned mid-ranks.

3.2. End of incubation

The end of incubation is calculated using the impingement-damage model for a commercial polyurethane topcoat applied to glass fibre-epoxy specimens (Bech et al., 2022). The volume of impinged water (H) hitting the blade during a time step causes incremental damage. Each damage increment is counted, and using Palmgren-Miner's summation, the accumulated dimensionless damage index is integrated over the time step. The impact velocity (V) is measured and the impinged water (H) calculated from the whirling arm test. The empirical relationship between V and H for the end-of-incubation observations provides a VH-curve (Bech et al., 2022). The VH-curve characterises how quickly the material wears down for impinged water.

https://doi.org/10.5194/wes-2026-225
Preprint. Discussion started: 25 November 2026
© Author(s) 2026. CC BY 4.0 License.



eawe european academy of wind energy
Open Access WIND ENERGY SCIENCE DISCUSSIONS

The tangential velocity is a function of the radial position along the blade and rpm. Due to aerodynamic effects, the impact velocity of hydrometeors on the leading edge of a blade is lower than idealized analyses would suggest, as droplets slow down as they approach the airfoil, reducing their impact speeds. The aerodynamic effects cause greater speed reduction for smaller droplets than for larger ones. An aerodynamic slowdown model that includes airfoil dimensions, droplet size, and shapes is applied (Barfknecht and von Terzi, 2024). The rate of damage scales non-linearly with impact velocity. Therefore, the difference in impact velocity during a full rotor sweep, with higher impact velocity during upward motion than downward, is included (Keegan et al., 2013). End-of-incubation results for the tips of the reference turbines are calculated, not along the span or chord.

The end of incubation at the eight sites is calculated from 10 years of data using time-series analysis. The values for each year are recorded. The analysis aims to quantify the variation in the end of incubation between years compared to the 10-year value.

3.3 Erosion safe operation (ESO)

Wind speed and rain intensity are the two variables predicting leading-edge erosion. Under normal operating conditions, a wind turbine runs at its nominal rotor speed regardless of the weather. However, under an ESO strategy, the turbine is curtailed during periods of intense rainfall to minimize blade damage. The optimal ESO strategy is governed by the specific weather conditions, blade materials, and turbine tip-speed curve.

The optimal ESO strategy balances extended blade life against potential AEP losses. To quantify this trade-off, a performance metric is defined as the ratio of the marginal change in power to the marginal change in the damage accumulation rate. The cost of coating life at any given timestep is then calculated using the partial derivatives of power and damage (Madsen et al., 2026; Hasager et al., in review). The power is derived from power coefficient (C_p) tables. C_p tables are available for each of the three reference turbines. The power curves for each of the reference turbines are used to calculate the power loss. The framework, developed by Madsen et al. (2026), evaluates the efficiency of ESO by generating a continuous range of optimal strategies along a Pareto front. This front represents a set of solutions in which no single option outperforms any other across all metrics, providing a comprehensive basis for decisionmakers to select their preferred balance between damage and AEP loss.

3.4 Empirical method for assessing the end of incubation and ESO efficiency

The end of incubation and ESO efficiency for all of Europe is calculated from 9 years of data using an empirical method. The time series method requires substantial computational resources. Therefore, a faster method is selected. The empirical method groups the rain intensity and wind speed data into bins (Visbech et al., 2025). The wind speeds are binned into 100 partitions from wind turbine cut-in to cut-out speeds, while the rain intensity is binned into 60 partitions from 0.001 mm to 100 mm. Note the lower value of rain intensity should be smaller than the resolution of the data (0.01 mm h^{-1} for IMERG) and cannot be zero. The computation time using the empirical method is roughly 15 hours for ~300,000 grid cells on a computational node

https://doi.org/10.5194/wes-2026-225
Preprint. Discussion started: 25 November 2026
© Author(s) 2026. CC BY 4.0 License.



eawe european academy of wind energy
Open Access WIND ENERGY SCIENCE DISCUSSIONS

in DTU's Sophia HPC cluster. The utilized hardware is described in the docs: https://dtu-sophia.github.io/docs/hardware/. The maps are based on 9 years of data during 2014-2022 with a grid resolution of 3 km by 3 km.

The performance of the time series and empirical methods is tested with a 10-year time series at Risø site. The comparison result is shown in Fig. 3. End of incubation is noted at 0% annual energy production (AEP) loss in Fig. 3. Applying erosion safe operation extends the lifetime for a given percentage AEP loss (section 3.4).

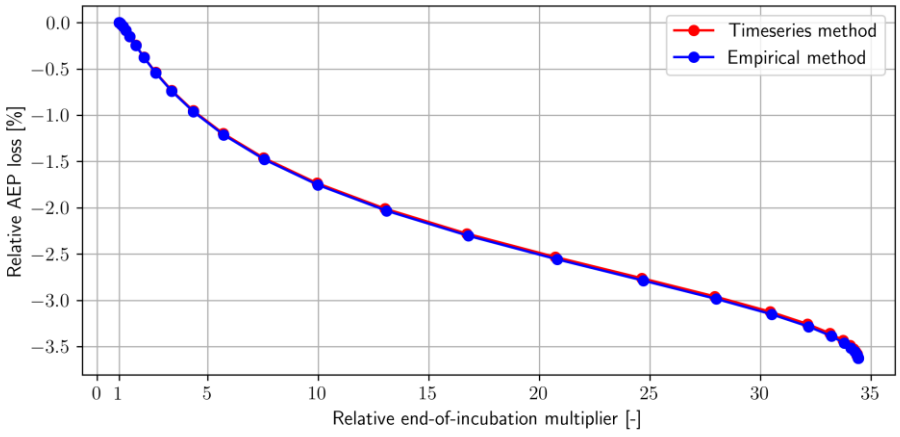


Figure 3: Erosion safe operation efficiency Pareto front for Risø site based on 10 years of 30- minute values for an IEA 15 MW turbine comparing the time series and empirical methods.

3.5 Probabilistic quantification on the end of incubation and ESO efficiency

Probabilistic quantification of the variability in the end of incubation and ESO efficiency follows the method introduced in Madsen et al. (2026). It is based on a probabilistic Pareto fronts approach driven by Monte Carlo simulations (Hasager et al., in review). In the current study material damage is assessed deterministically and only uncertainty on weather is quantified. Concurrent pairs of wind speed and rain intensity are randomly sampled with replacement from a multi-year historical time series. For each simulation, the total number of sampled data points aggregates to exactly one year of observations. This random selection process effectively captures annual weather variability. The uncertainty sampling analysis for weather conditions is conducted via Monte Carlo simulation with 100 realizations. The synthetic year samples are used to evaluates performance variations, with a focus on behaviour around the Pareto front.

3.6 Reference turbines

Three reference wind turbines are selected for the study: NREL 5MW, DTU 10 MW, and IEA 15 MW. Table 2 provides relevant details such as hub height, rotor diameter, cut-in, rated, and cut-out speeds, maximum tip speed, and minimum and maximum rpm. The tip speed curve and rpm are used in the damage calculation while the droplet slowdown method also

https://doi.org/10.5194/wes-2026-225
Preprint. Discussion started: 25 November 2026
© Author(s) 2026. CC BY 4.0 License.



eawe european academy of wind energy
Open Access WIND ENERGY SCIENCE DISCUSSIONS

includes blade airfoil. Erosion safe operation calculation additionally depends on rpm minimum, rpm maximum, cut-in, rated and cut-out wind speed.

Table 2: Wind turbines specifications.

Turbine	Hub height (m)	Rotor diameter (m)	Cut-in ($m\ s^{-1}$)	Rated ($m\ s^{-1}$)	Cut-out ($m\ s^{-1}$)	Max. tip speed ($m\ s^{-1}$)	Min. (rpm)	Max. (rpm)
NREL 5 MW	90	126	3	11.4	25	80	6.9	12.1
DTU 10 MW	119	178.3	4	11.4	25	90	6.0	9.6
IEA 15 MW	150	240	3	10.6	25	95	5.0	7.56

4. Results

4.1 Weather statistics at eight sites

Weather statistics for the eight selected sites are presented below, based on IMERG and NEWA during 2014-2023. Average annual precipitation and associated likelihood of the precipitation in the form of liquid and solid fractions and mean wind speeds are shown in Fig. 4.

Buseco, located in NW Spain, has the highest average annual precipitation (~1,200 mm), nearly all of it falling as liquid. In contrast, Båtskär in Finland, in the northern Baltic Sea, has the lowest average annual precipitation (~600 mm), of which ~10% is in the solid fraction. Alaiz, inland in Spain, has the lowest average wind speed (7.1 $m\ s^{-1}$), while Moray East in the UK North Sea has the highest (9.7 $m\ s^{-1}$).

The values on annual average rainfall and average wind speeds are listed in Table 3. Table 3 also lists the Spearman coefficient for all sites, showing high values for Buseco, Moray East, and Båtskär and low values for Levenmouth and Rézentières. High Spearman coefficients indicate high rain during windy conditions. High values indicate high-dependency sites on the rain-wind speed climate while near-zero show low-dependency sites.

https://doi.org/10.5194/wes-2026-225
Preprint. Discussion started: 25 November 2026
© Author(s) 2026. CC BY 4.0 License.

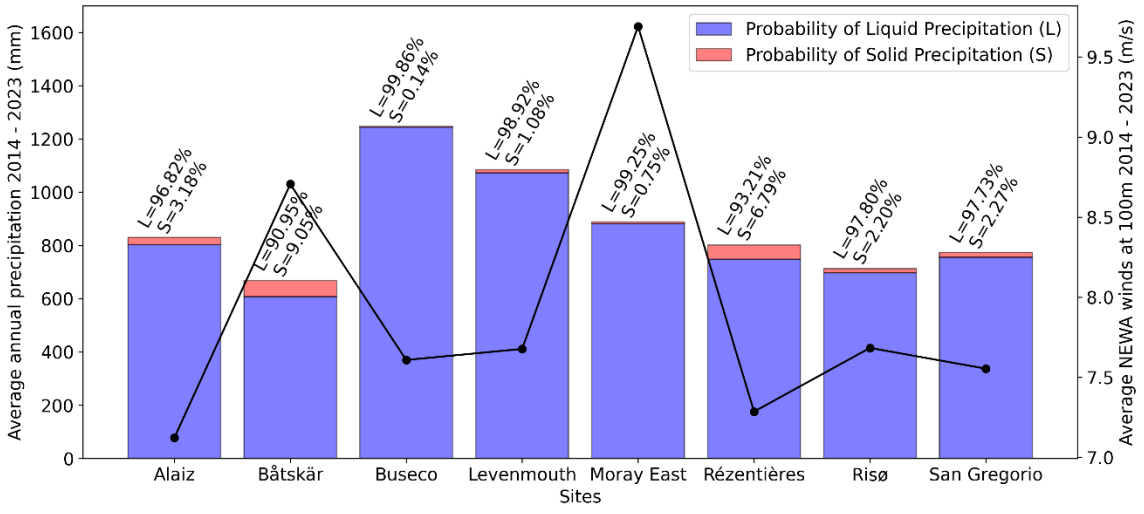


Fig. 4. Annual average rainfall at eight sites based on IMERG during 2014-2023, probability of liquid and solid fractions, and mean wind speed at 100 m height from NEWA.

Table 3: IMERG average annual rainfall and NEWA average wind speed at 100 m height and Spearman correlation during 2014-2023.

Site	Average annual rainfall (mm)	Average wind speed (m/s)	Spearmann correlation (-)
Alaiz	803	7.1	0.10
Båtskär	607	8.7	0.16
Buseco	1245	7.6	0.17
Levenmouth	1073	7.7	0.06
Moray East	882	9.7	0.17
Rézentières	748	7.3	0.07
Risø	698	7.7	0.11
San Gregorio	756	7.5	0.09

4.2 Weather statistics for Europe

Weather statistics for Europe are presented below, based on IMERG and NEWA during 2014-2022. Average annual rainfall, the probability of liquid precipitation, and the fraction of low-quality data in IMERG are shown in Fig. 5a, c, and d, respectively. Annual average rainfall ranges from below 500 mm to more than 2,500 mm. NW Europe is generally wetter. The probability of liquid precipitation is high over the seas, while inland, at northern and mid-latitudes, including the Alps, solid

https://doi.org/10.5194/wes-2026-225
Preprint. Discussion started: 25 November 2026
© Author(s) 2026. CC BY 4.0 License.

precipitation is frequent. The quality of IMERG data is shown in Fig. 5d. Note that the fraction of low-quality data is higher where solid precipitation occurs frequently. The maps are digitally accessible (Vinod et al., 2026).

Average wind speeds from NEWA are shown in Fig. 5b. Higher winds are noted in the Atlantic Ocean and the North Sea than inland.

The Spearman correlation is calculated from the IMERG and NEWA concurrent time series at each grid point and is shown in Fig. 6. The highest correlations are observed in the Norwegian Sea and northwest of the Scottish coast. Interestingly, most of Europe exhibits a positive Spearman correlation. However, the Alps and other inland regions show slightly negative values.

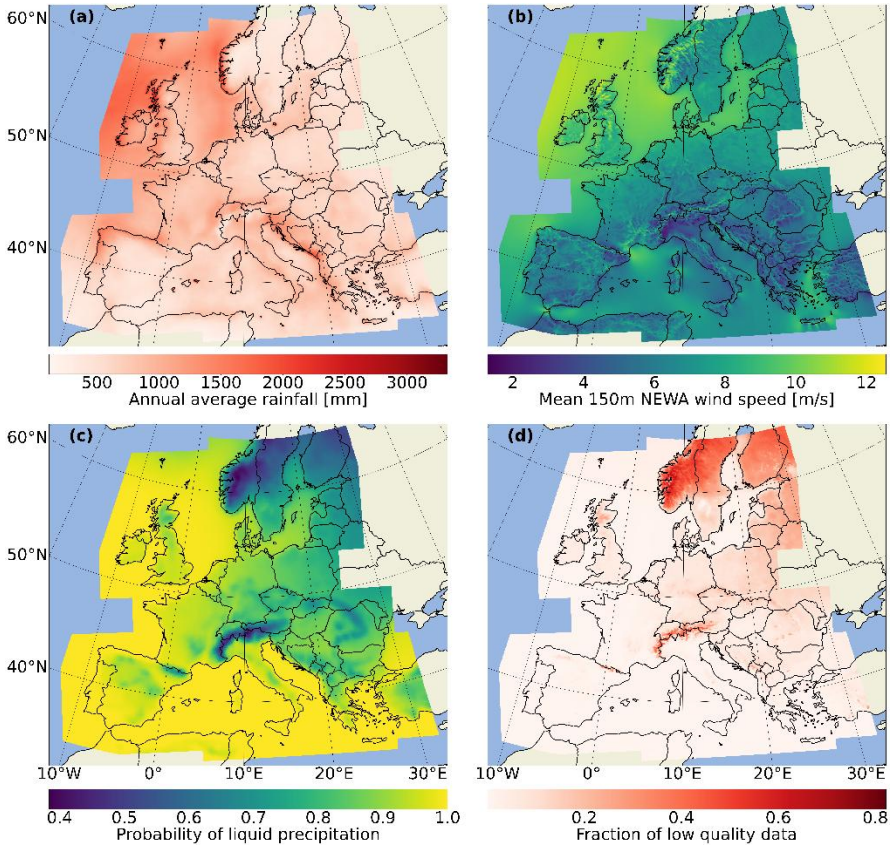


Figure 5: a) IMERG annual average rainfall, b) NEWA average wind speed at 150 m, c) probability of liquid precipitation from IMERG, d) fraction of low-quality data from IMERG during 2014-2022.

https://doi.org/10.5194/wes-2026-225
Preprint. Discussion started: 25 November 2026
© Author(s) 2026. CC BY 4.0 License.

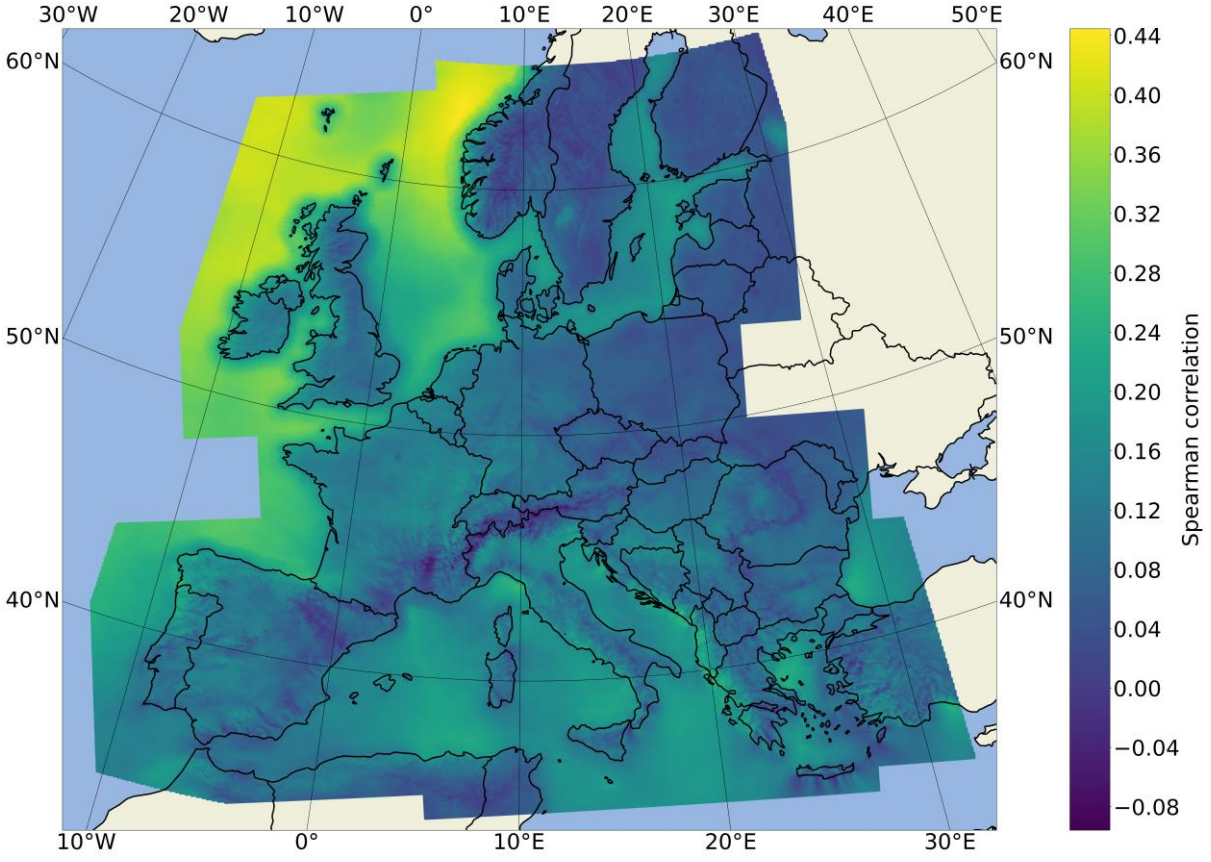


Figure 6: Spearman correlation for IMERG rainfall and NEWA 150m wind speeds during 2014-2022.

4.3 End of incubation at eight sites

The end of incubation is calculated using 10 years of IMERG and NEWA data at the eight sites. A DTU 10 MW turbine is assumed to have been operating at each site during the period. The end-of-incubation mean value over 10 years ranges from ~4 years at Buseco and ~5 years at Moray East to ~12 years at Rézentières.

The end of incubation is estimated for each year to investigate interannual variability. The minimum and maximum incubation-end values for each year are listed in Table 4. The percentage variation between the individual end-of-incubation-year minimum and maximum is, on average across the 8 sites, ~100% and up to ~135% (Rézentières).

Table 4: Year-to-year variability in the end of incubation during 10 years, mean, minimum and maximum for 10 individual years, and percentage variation minimum to maximum based on IMERG rainfall and NEWA wind speed during 2014-2023, assuming a DTU 10 MW turbine was installed at each site.

https://doi.org/10.5194/wes-2026-225
Preprint. Discussion started: 25 November 2026
© Author(s) 2026. CC BY 4.0 License.



eawe european academy of wind energy
Open Access WIND ENERGY SCIENCE DISCUSSIONS

Site	Mean (yrs)	Min. (yrs)	Max. (yrs)	Percentage variation min-to-max (%)
Alaiz	8.8	7.0	10.1	45
Båtskär	8.2	5.2	11.8	128
Buseco	4.0	2.7	5.3	98
Levenmouth	6.5	4.2	8.6	106
Moray East	5.1	4.0	7.3	81
Rézentières	11.7	8.7	20.4	135
Risø	9.4	7.0	15.5	122
San Gregorio	8.3	6.5	11.2	72

4.4 End of incubation for Europe

The end of incubation, calculated across Europe, is based on 9 years of concurrent measured rainfall from IMERG and modelled wind speed from NEWA every 30 minutes. Three reference turbines are assumed to have been installed in each grid cell. The atlas of erosion risk is shown in Fig. 7. The incubation period is shortest for the IEA 15 MW turbine due to higher hub-height winds, a lower minimum rpm, a lower rated speed, and a higher tip speed compared to the other two reference turbines. In contrast, the NREL 5 MW has the lowest hub height and tip speed, while the DTU 10 MW is in between.

The atlas on erosion risk displays much spatial variability. The atlas shows the shortest end of incubation at sea in the northwest and the longest end of incubation inland.

NREL 5 MW can operate for far more than 20 years at most land sites without reaching the end of incubation, but if located in the Atlantic Ocean or the North Sea, it would show the end of incubation at ~7 to 8 years (Fig. 7a).

DTU 10 MW can operate for more than 20 years only inland, while at sea, the incubation period would range from ~5 to 12 years in the Atlantic, North Sea, Baltic Sea, and most of the Mediterranean Sea. The longest incubation periods are seen in the Alps, parts of Norway, Sweden, Finland, Romania and the Balkans (Fig. 7b). However, in mountainous areas and in eastern Europe, the end of incubation may be underestimated as IMERG data have a high fraction of low-quality data there (cf. Fig. 5d). Furthermore, modelled winds in highly complex regions are less reliable than in flatter terrain.

IEA 15 MW indicates that the incubation period is shorter than ~6 years in extended offshore areas and shorter than ~12 years on land in most of Europe. Longer than ~20 years is noted in mountainous areas, the Alps, parts of Norway, Sweden, Romania, and the Balkans (Fig. 7c).

https://doi.org/10.5194/wes-2026-225
Preprint. Discussion started: 25 November 2026
© Author(s) 2026. CC BY 4.0 License.

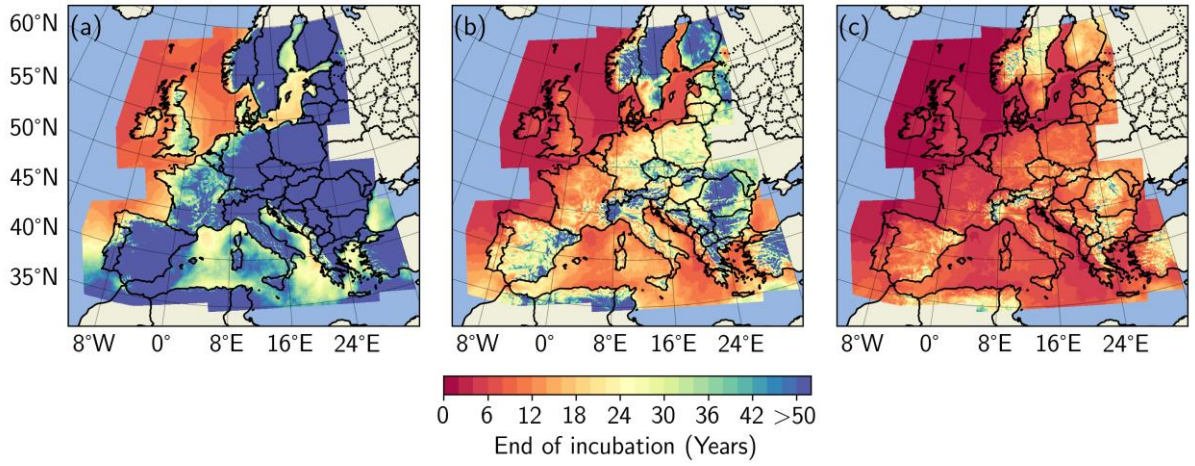


Figure 7: End of incubation based on IMERG rainfall and NEWA wind speeds during 2014-2022, assuming a reference turbine was operating in each grid cell for a) NREL 5 MW turbine, b) DTU 10 MW turbine, c) IEA 15 MW turbine.

4.5 Erosion safe operation (ESO) efficiency at eight sites

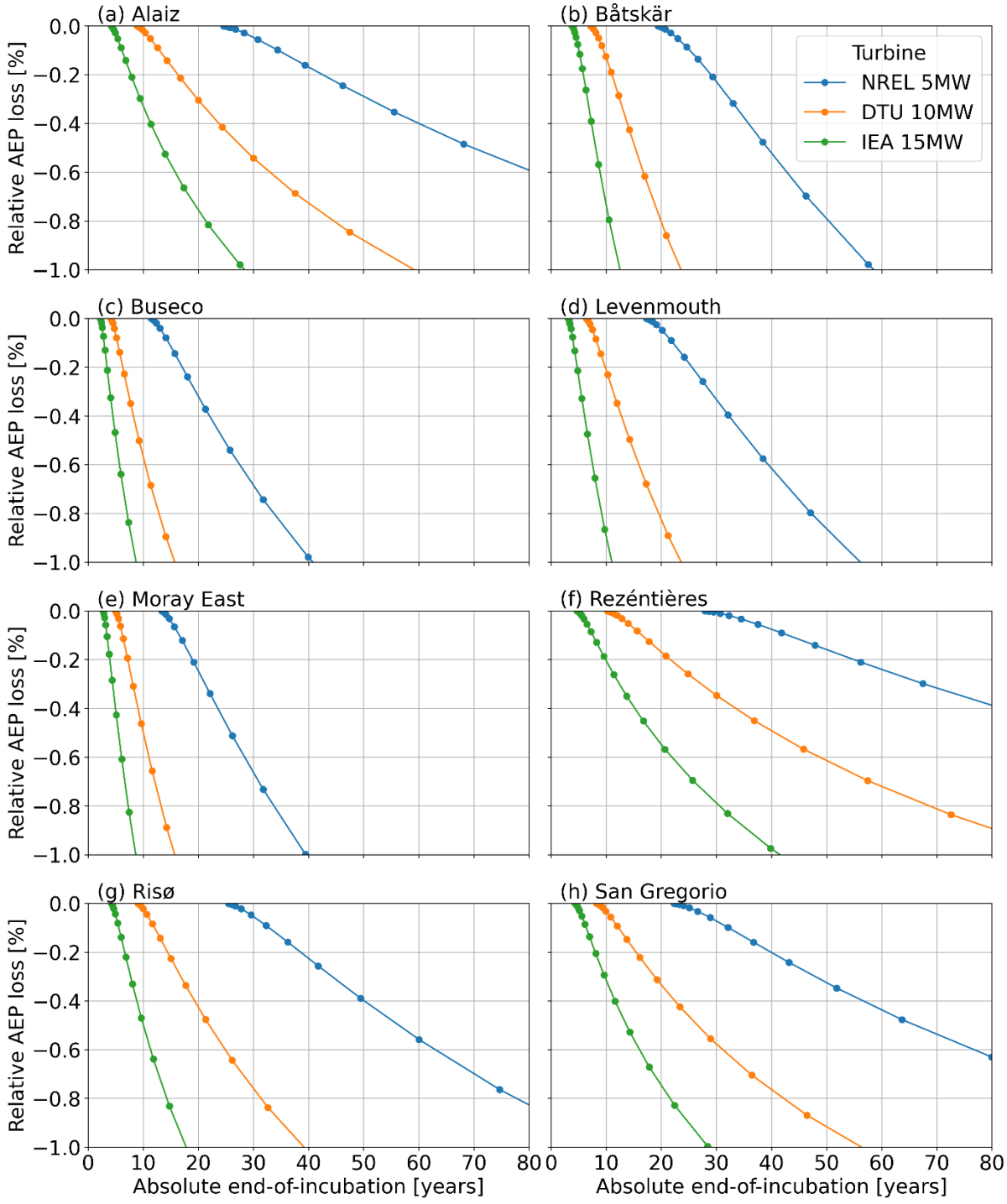
ESO efficiency is investigated at eight sites for the period 2014 to 2023 based on IMERG rainfall and NEWA, assuming three reference turbines, NREL 5 MW, DTU 10 MW turbine, and IEA 15 MW, were installed at each location during the period. The erosion-safe operation Pareto fronts are displayed in Fig. 8, indicating the absolute end-of-incubation for AEP losses ranging from 0 to 1%. At all sites, the incubation period is longest for NREL 5 MW, intermediate for DTU 10 MW, and shortest for IEA 15 MW, as expected.

For Alaiz, the end of incubation is beyond 20 years for NREL 5 MW, ~9 years for DTU 10 MW, and ~6 years for IEA 15 MW under normal operation, i.e., erosion-safe operation is not applied. Turbines are operating full speed in all conditions, independent of rain events (Fig. 8a). This corresponds to an AEP loss of 0%. Applying ESO efficiently would reduce turbine speed during the most damaging intervals, thereby increasing the time to the end of incubation and causing AEP loss. DTU 10 MW would reach ~20 years end of incubation for ~ 0.3% AEP loss, while IEA 15 MW would reach ~ 20 years end of incubation for ~ 0.8% AEP loss.

Buseco and Moray East show very steep Pareto front curves, indicating a harsh erosion climate in which none of the three reference turbines would reach the 20-year end of incubation without ESO (Figs. 8c, e). In contrast, sites with milder erosion climates include Rézentières, Alaiz, San Gregorio, and Risø, showing flatter Pareto front curves, and NREL 5 MW shows the end of incubation beyond 20 years (Figs. 8f, a, h, g). At Båtskär and Levenmouth, NREL 5 MW would nearly reach 20 years of end of incubation without ESO.

Examining ESO efficiency in more detail, it may be noted that the IEA 15 MW shows ~5 years at the end of incubation without ESO at Rézentières and Risø. The climate at Rézentières would allow ~20 years of end-of-incubation for ~0.6% AEP, while at Risø it would require more than ~1% AEP loss (Fig. 8f, g). In summary, flatter Pareto fronts indicate a longer incubation period for limited AEP loss.

https://doi.org/10.5194/wes-2026-225
Preprint. Discussion started: 25 November 2026
© Author(s) 2026. CC BY 4.0 License.



https://doi.org/10.5194/wes-2026-225
Preprint. Discussion started: 25 November 2026
© Author(s) 2026. CC BY 4.0 License.



eawe european academy of wind energy
Open Access WIND ENERGY SCIENCE DISCUSSIONS

305 **Figure 8: Erosion safe operation efficiency Pareto front showing relative AEP loss and absolute end of incubation based IMERG rainfall and NEWA wind speed during 2014-2023, assuming at each site reference turbines NREL 5 MW, DTU 10 MW and IEA 15 MW turbines were operating a) Alaiz, b) Båtskär, c) Buseco, d) Levenmouth, e) Moray East, f) Rézentières, g) Risø, and h) San Gregorio.**

310

4.6 Erosion safe operation (ESO) efficiency for Europe

ESO efficiency for Europe is calculated assuming the three reference turbines were operating in each grid cell during the 9 years from 2014 to 2022. Considering it would be acceptable to curtail the turbines during the most erosive events for an AEP loss of 0.2%, the expected extension of the end of incubation is shown in Figs. 9a, b, c. Results for a 0.4% AEP loss, showing
315 the expected extension at the end of incubation, are displayed in Figs. 9d, e, f.

The six maps at the end of incubation extension show large geographical variation (Fig. 9). For the NREL 5 MW turbine, most land sites show more than 20 years of end-of-incubation extension for 0.2% AEP loss. The relevance of ESO at land sites for the NREL 5 MW turbine is low, as the end of incubation without curtailment is more than 20 years on land (Fig. 7a). In the Atlantic and North Seas, the end of incubation for the NREL 5 MW turbine is shorter than 20 years. Extension of the end of
320 incubation could be relevant, showing ~3 to ~6 years extension for 0.2% AEP loss.

As expected, the extension of the end of incubation is shorter for the DTU 10 MW turbine than for the NREL 5 MW turbine, and even shorter for the IEA 15 MW turbine. Again, considering whether ESO is relevant for a site, the first step is checking the end of incubation without curtailment (Fig. 7b, c), and comparing with the potential extension of end of incubation for a loss of, e.g., 0.2 or 0.4% AEP loss (Fig. 9b, c, e, f).

https://doi.org/10.5194/wes-2026-225
Preprint. Discussion started: 25 November 2026
© Author(s) 2026. CC BY 4.0 License.

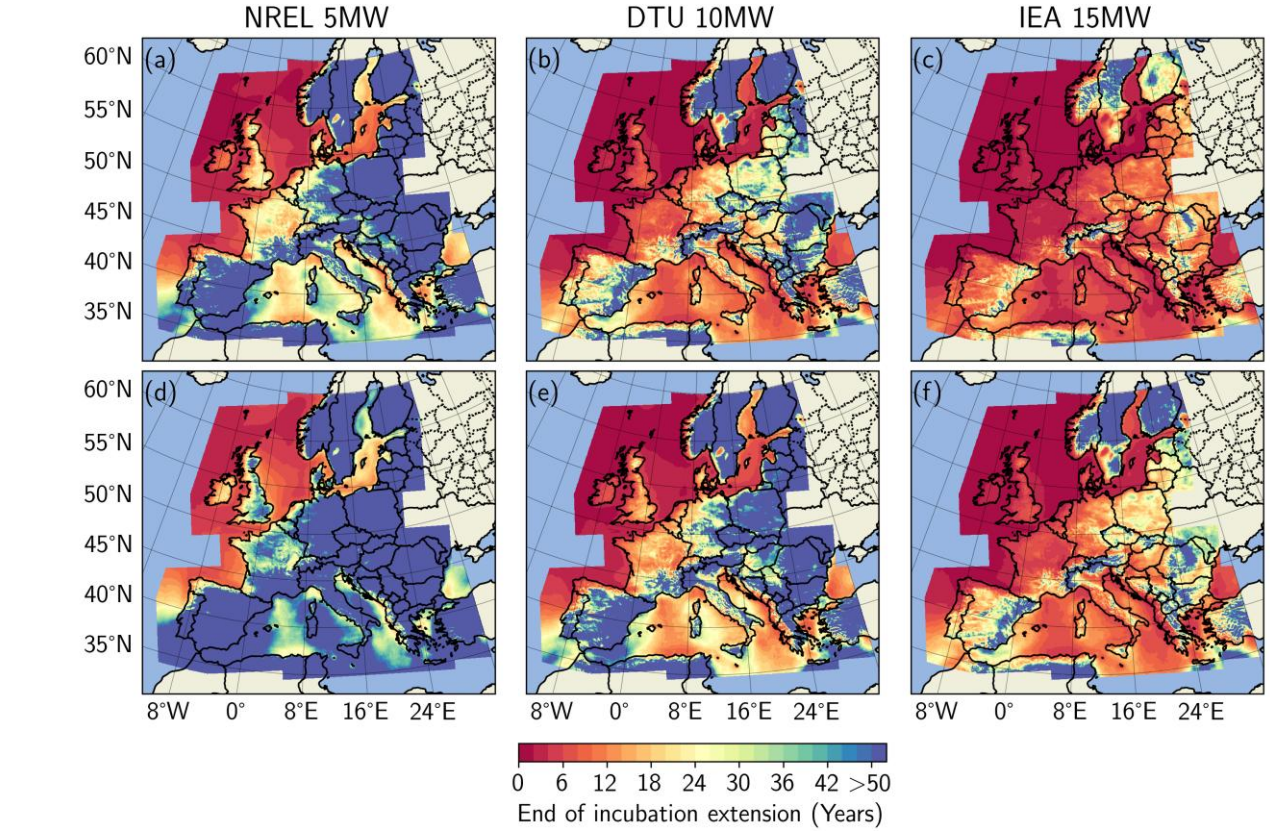


Fig. 9. Erosion safe operation extension of end of incubation based on IMERG rainfall and NEWA wind speeds observations during 2014-2022 for a) NREL 5 MW, b) DTU 10 MW, c) IEA 15 MW for AEP loss at 0.2%, and d), e) and f) for AEP loss at 0.4%, respectively.

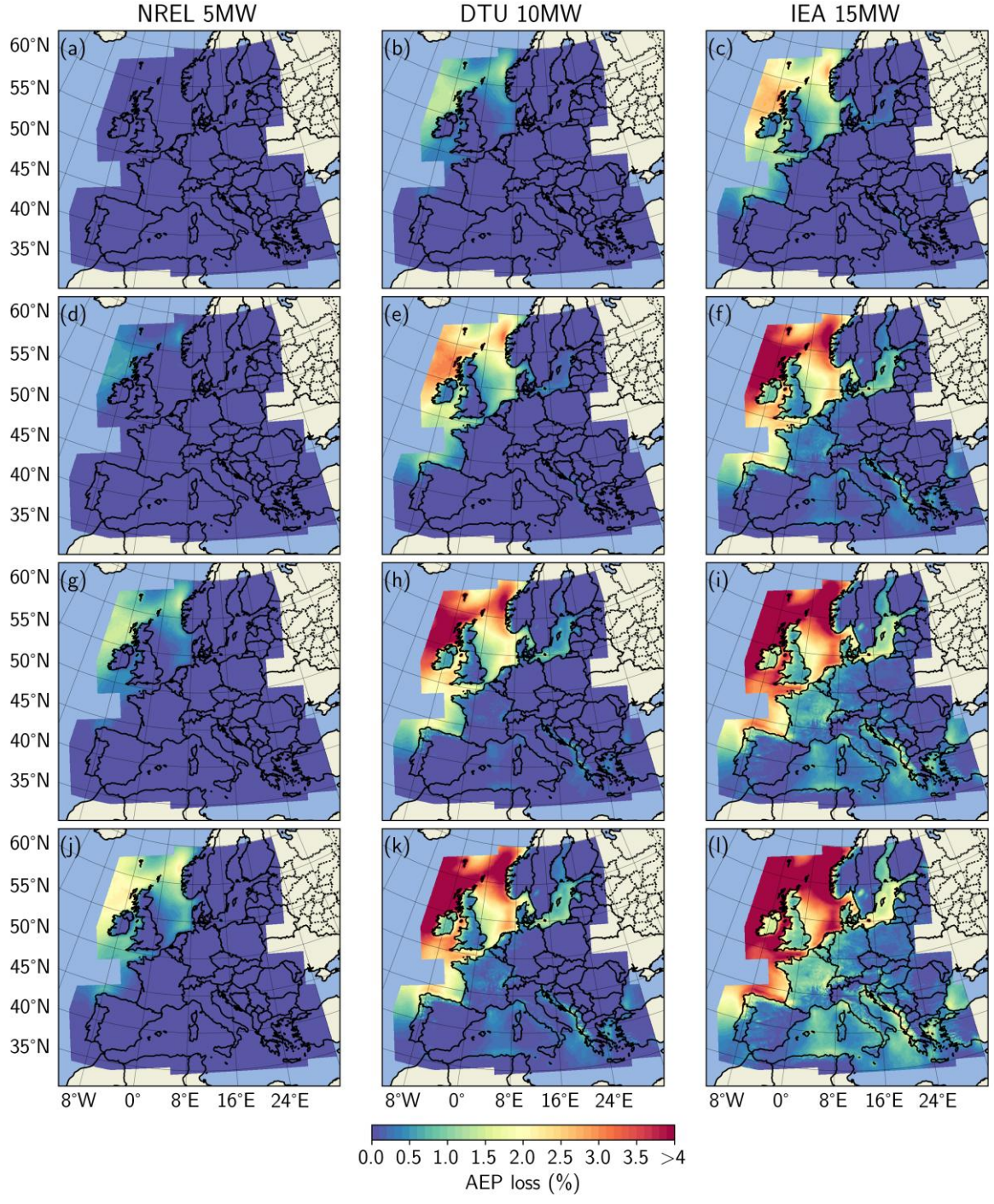
An alternative way of displaying ESO efficiency is shown in Fig. 10. The calculation is performed for the same period and the same three turbines as above. The result shows the AEP loss required to ensure 5-, 10-, 15-, and 20-year end of incubation when applying ESO efficiently.

NREL 5 MW turbines would reach more than 5 years' end of incubation in the entire Europe without ESO (Fig.10a). On land, NREL 5MW would reach 20 years end of incubation without ESO but would require up to ~2% AEP loss in parts of the Atlantic Ocean and North Sea (Fig.10j).

On land, DTU 10 MW turbines would exceed 5 years End of incubation without ESO (Fig. 10b). To reach 10 years end of incubation, ESO would be required in western Ireland and the western UK (Fig. 10e). To reach 20 years end of incubation, ESO would be required offshore in various locations and along western coastlines in many countries (Fig. 10k).

https://doi.org/10.5194/wes-2026-225
Preprint. Discussion started: 25 November 2026
© Author(s) 2026. CC BY 4.0 License.

340 IEA 15 MW turbines onshore would reach 5 years end of incubation without ESO at most sites, except exposed western coastal regions (Fig.10c). The AEP loss required to reach 20 years of end of incubation is below ~2% in most onshore regions. In contrast, in parts of the Atlantic Ocean and the North Sea, AEP losses exceed 4% (Fig. 10l).



https://doi.org/10.5194/wes-2026-225
Preprint. Discussion started: 25 November 2026
© Author(s) 2026. CC BY 4.0 License.



eawe european academy of wind energy
Open Access WIND ENERGY SCIENCE DISCUSSIONS

345 **Fig. 10. AEP loss (%) assessed using optimal erosion safe operation for achieving 5 years end of incubation: a), b), c); 10 years end of incubation: d), e), f); 15 years end of incubation: g), h), i); and 20 years end of incubation: j), k), l) for NREL 5 MW turbine (left column), DTU 10 MW turbine (middle column) and IEA 15 MW turbine (right column) based on IMERG rainfall and NEWA wind speeds during 2014-2022.**

350 **4.7 Probabilistic erosion safe operation (ESO) efficiency Pareto fronts results at eight sites**

The uncertainty in the ESO efficiency Pareto fronts is investigated assuming that DTU 10 MW turbines were operating at each of the eight sites during the period 2014 to 2023. The IMERG rain intensity and NEWA wind speed concurrent pairs of data were randomly selected from the 10-year time series, with the total number of sampled points totalling one year of observations. One hundred Monte Carlo simulations were run at each site to quantify probabilistic uncertainty of the Pareto fronts.

355 The frequency distribution of ESO efficiency Pareto fronts is shown in Fig. 11 for the eight sites. For AEP loss of 0%, corresponding to normal operation without curtailment, the end of incubation varies across sites. The shortest incubation period is noted for Buseco, the longest for Rézentières. The result aligns with the results at the end of incubation in Table 4, which uses the entire time series, even though probabilistic random sampling is not expected to yield the same values.

The steepness of the Pareto fronts varies between sites. The steepest Pareto front is observed for Buseco, while the flattest is

360 for Rézentières (Fig. 11). The steepness of the Pareto fronts aligns with the results based on the whole series (Fig. 8).

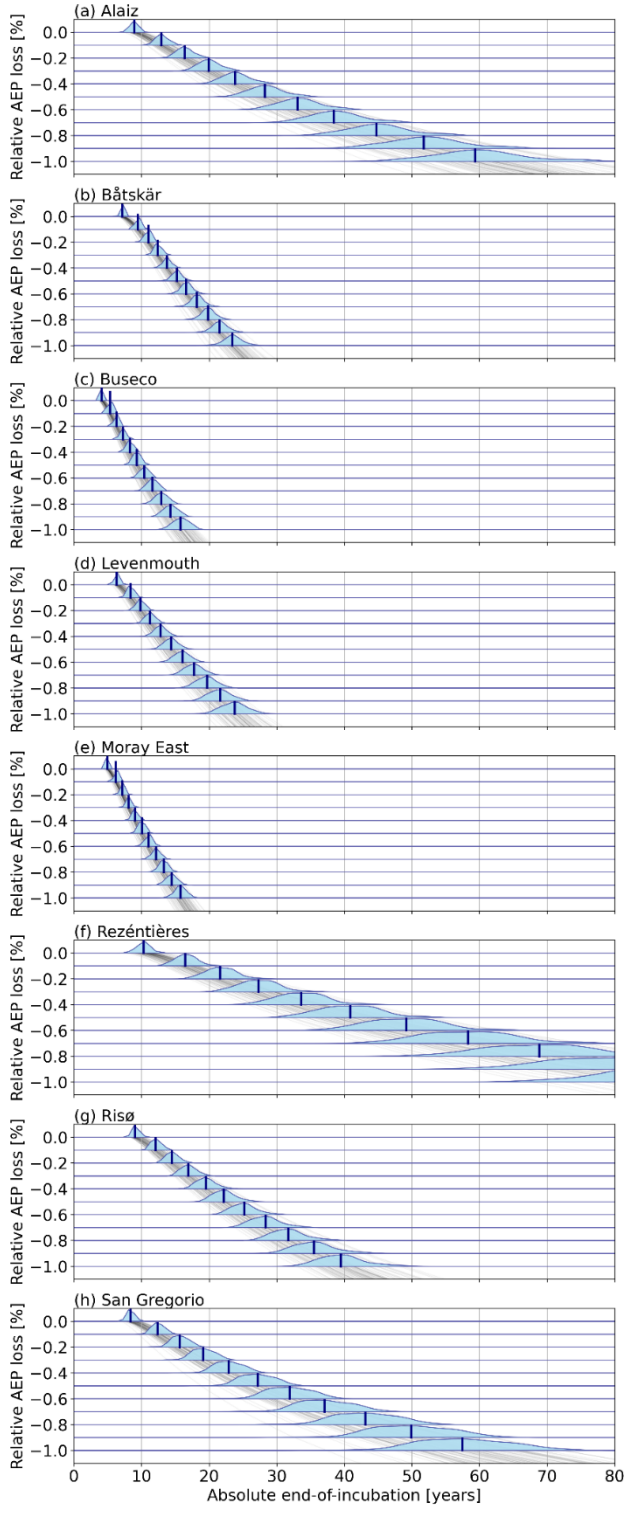
The end of incubation frequency distributions broadens with increasing AEP losses and are shown for AEP losses at 0.1% intervals from 0 to 1% at all sites (Fig. 11). The frequency distribution values listed in Table 5 include median, minimum, maximum, and the difference between maximum and minimum for AEP losses at 0, 0.2 and 0.4%. The smallest difference between the maximum and minimum ends of the incubation is noted for 0% AEP loss for Moray East (1.0 year) and for 0.4%

365 AEP loss (2.0 years), i.e., a doubling of the range between the two frequency distributions. For Buseco, the frequency distribution ranges are 1.4 years for 0% AEP loss and 2.4 years for 0.4% AEP loss, i.e., less than a doubling between the two distributions. In contrast, Alaiz and San Gregorio show a tripling and a quadrupling, respectively, in the range of the frequency distributions for 0% and 0.4% AEP loss.

In general, the probabilistic approach can be used to estimate the likelihood on End of incubation and ESO efficiency. The

370 current analysis assesses the probability that the weather over the period yields the reported End of incubation values but do not consider material uncertainties.

https://doi.org/10.5194/wes-2026-225
Preprint. Discussion started: 25 November 2026
© Author(s) 2026. CC BY 4.0 License.



https://doi.org/10.5194/wes-2026-225
Preprint. Discussion started: 25 November 2026
© Author(s) 2026. CC BY 4.0 License.



eawe european academy of wind energy
Open Access WIND ENERGY SCIENCE DISCUSSIONS

Fig. 11. Frequency distribution of erosion safe operation efficiency Pareto fronts showing relative AEP loss and absolute end of incubation for 100 Monte Carlo simulations and indicating the median value (black vertical lines) uncertainties, based on IMERG rain intensity and NEWA wind speed for 2014 to 2023 and assuming DTU 10 MW turbines were operating at a) Alaiz, b) Båtskär, c) Buseco, d) Levenmouth, e) Moray East, f) Rézentières, g) Risø, and h) San Gregorio.

Table 5. Erosion safe operation efficiency listing end of incubation uncertainty in the form of median, minimum, maximum and difference between minimum and maximum based on IMERG rain intensity and NEWA wind speed for 2014 to 2023 for normal operation (AEP loss 0%) and curtailment (AEP loss 0.2% and 0.4%), assuming DTU 10 MW turbines were operating at each site.

Total uncertainties	AEP loss (%)	End of incubation (years)			
		Median	Minimum	Maximum	Difference max-min
Alaiz	0	9.0	7.4	10.6	3.2
	0.2	16.3	13.8	19.8	6.0
	0.4	23.6	19.9	29.8	9.9
Båtskär	0	7.3	6.6	8.4	1.8
	0.2	11.0	9.9	12.5	2.6
	0.4	13.8	12.1	15.7	3.6
Buseco	0	4.2	3.6	5.0	1.4
	0.2	6.3	5.3	7.5	2.2
	0.4	8.3	7.2	9.6	2.4
Levenmouth	0	6.4	5.7	7.5	1.8
	0.2	9.8	8.2	11.5	3.3
	0.4	12.8	10.1	14.7	4.6
Moray East	0	5.0	4.5	5.4	0.9
	0.2	7.2	6.5	7.9	1.4
	0.4	9.1	8.2	10.2	2.0
Rézentières	0	10.4	8.2	12.7	4.5
	0.2	21.5	16.9	26.4	9.5
	0.4	32.9	26.8	39.8	13.0
Risø	0	9.1	8.2	10.6	2.4
	0.2	14.5	12.5	16.9	4.4
	0.4	19.3	16.1	22.5	6.4
San Gregorio	0	8.5	7.4	9.8	2.4
	0.2	15.4	13.1	20.2	7.1

https://doi.org/10.5194/wes-2026-225
Preprint. Discussion started: 25 November 2026
© Author(s) 2026. CC BY 4.0 License.



eawe european academy of wind energy
Open Access WIND ENERGY SCIENCE DISCUSSIONS

	0.4	22.4	18.0	28.9	10.9

385

5. Discussion

5.1 Weather conditions

390 The wind speeds from NEWA, combined with rainfall from IMERG, during 2014 to 2022, show a positive Spearman correlation across most of Europe. Previous results include Visbech et al. (2025), which cover the British Isles and surrounding seas and identified a positive correlation across most of the region using a Copula parameter. It is possible to describe a site using correlation to assess whether it is a high-dependency site (i.e., high rainfall is more likely during high wind speed) or a low-dependency site.

395 The Spearman correlation shows the largest positive values offshore in the Norwegian Sea, exceeding 0.44, while the largest negative values are found in the Alps, at ~-0.08. The results in the Alps are called into question due to a high fraction of low-quality IMERG data. Furthermore, modelled winds in highly complex regions are less trustworthy than in flatter terrain (Dörenkämper et al., 2020). IMERG suffers from a high fraction of low-quality data in parts of Norway, Sweden, and Finland. These regions and the Alps are all prone to high fractions of solid precipitation. The results based on NEWA and IMERG 400 combined are likely less accurate in these regions than elsewhere in Europe. In order to reduce bias, IMERG Final Run is calibrated to the Global Precipitation Climatology Centre (GPCC) gauge analysis at monthly scale over land only. Offshore, it relies on satellite retrievals anchored to the GPCP climatology. Monthly totals are therefore more directly constrained onshore, while sub-monthly intensities are not gauge-constrained in either domain (Huffman et al., 2023). The variability in number of gauges used for gauge correction vary across Europe (Ivanova, 2025).

405 Interannual variation at the end of incubation is ~100% on average across the eight sites investigated. The results compare well with previous studies (Pryor et al., 2025; Hasager et al., in review). A longer series would be preferable to assess the end of incubation. Ongoing climate change means that past conditions may not be fully representative of the future (IPCC, 2023). At the Risø site, changes in precipitation and wind speed were examined using a 19-year, non-continuous time series, which showed a wetter climate in recent years at Risø (Hasager et al., in review).

410

5.2 End of incubation

The European maps at the end of incubation for the three reference turbines show large variations between the turbines. The variations at the end of incubation among the three reference turbines are due to differences in their hub height, minimum rpm, rated speed, and tip speed. The same three reference turbines were selected for mapping leading-edge erosion in the UK 415 (Visbech et al., 2025) and Japan (Sakai et al., 2026), and they showed similar variation in end-of-incubation between turbines.

https://doi.org/10.5194/wes-2026-225
Preprint. Discussion started: 25 November 2026
© Author(s) 2026. CC BY 4.0 License.

In the Netherlands, a study assuming a 1.5 MW turbine and DTU 10 MW also showed faster erosion from the larger turbine (Verma et al., 2021).

The end of incubation across Europe shows pronounced geographical variation. This is the first study to map all of Europe. Regional assessments of the Netherlands based on weather station observations (Verma et al., 2021) and mesoscale and large-eddy simulation modelling (Caboni and Dalum, 2025) show faster erosion offshore than inland, in agreement with our results. Regional assessment covering Scandinavia, based on NORA3 and ERA5, confirms spatial variability between offshore and land areas (Hannesdóttir et al., 2024). It should be noted that NORA3 provides precipitation values that are more trustworthy than IMERG over land in Norway and Sweden; thus, the end of incubation is expected to be better resolved from the 5-year study (Hannesdóttir et al., 2024) than in our study, which suffers from low-quality IMERG data over land in Norway and Sweden. Quantitative comparison among the different maps at the end of incubation is complicated by varying lengths and time-series periods.

Rainfall and wind speed vary across individual years, with an average of ~100% between the end-of-incubation minimum and maximum over 10 years at the eight selected sites. Using longer time series to assess interannual variability reveals even higher variation, ~170%, at the Risø site, based on 19 years of non-continuous rain-gauge data (Hasager et al., in review). Rain gauge data with up to 18 years of time series in the US (Pryor et al., 2025) and up to 16 years in Northern Europe (Hasager et al., 2021) show variation exceeding 100% between the minimum and maximum years at the end of incubation. The current maps, based on a 9-year series, could be improved with a longer series.

The probabilistic analysis of the end of incubation, performed by sampling concurrent pairs of rain intensity and wind speed at the eight sites using the 10-year time series, shows variability. The smallest difference between the minimum and maximum is ~1 year (Moray East), and the largest is ~5 years (Rézentières). The results indicate less temporal variability offshore than inland at a flat, high-altitude site.

Examining the end of incubation shows a much shorter duration at Moray East (~5 years) versus Rézentières (~12 years), assuming DTU 10 MW turbines were operating. Moray East has more rainfall and higher wind speed at 100 m height (~880 mm yr^{-1}, ~9.7 m s^{-1}) than Rézentières (~750 mm yr^{-1}, ~7.3 m s^{-1}). Furthermore, Moray East is a high-dependence site with a high Spearman correlation (~0.17), whereas Rézentières is a low-dependence site with a low Spearman correlation (~0.07).

Studies comparing the end of incubation using the time-series method versus the constant climate method, following DNV Recommended Practice (RP) (DNV, 2021), show that the latter yields a shorter end-of-incubation time (Castorrini et al., 2024; Visbech et al., 2025; Simon et al., 2026). The difference in end-of-incubation results between the two methods is expected to be greater for high-dependence sites than for low-dependence sites (Visbech et al., 2025). The Spearman correlation map indicates locations where the constant climate may be applicable and where locations are likely to be assessed as more erosive than with the time-series method. The higher the Spearman correlation, the more bias might be expected. Negative Spearman correlation locations may have a reverse assessment at the end of incubation. This has not been investigated in the current study and could be a future topic to examine.

https://doi.org/10.5194/wes-2026-225
Preprint. Discussion started: 25 November 2026
© Author(s) 2026. CC BY 4.0 License.



eawe european academy of wind energy
Open Access WIND ENERGY SCIENCE DISCUSSIONS

5.3 Erosion safe operation efficiency

The atlas at the end of incubation for the three reference turbines shows lifetimes of less than 20 years in the Atlantic Ocean for the NREL 5 MW, less than 20 years offshore and over extended land areas for the DTU 10 MW, and less than 20 years for most of Europe for the IEA 15 MW. The maps may be used to evaluate the risk of erosion for specific turbines and coating types. It should be kept in mind that the end of incubation constitutes a mild form of damage, hardly noticed in field surveys, where more severe damage categories are in focus (Mishnaevsky, 2021; Verma et al., 2021; Visbech et al., 2023; Sánchez et al., 2026). The duration from the end of incubation to more severe damage and breakthrough varies for coating types (Verma et al., 2021). In the current study, the end of incubation is used as a proxy for damage needing action. This action could be a repair solution or a way to reduce the risk of needing repair by curtailing the turbines during the most erosive events, thereby extending the time to the end of incubation.

The atlas on erosion safe operation (ESO) efficiency is provided with two metrics. The first metric is how much the end of incubation is expected to be extended if allowing 0.2% and 0.4% AEP loss for each of the three reference turbines. The maps show geographic variability. Due to non-linearities and variability in concurrent rain intensity and wind speed distributions, a simple doubling in extended end of incubation cannot be expected for each additional AEP loss increment. ESO efficiency Pareto fronts for the eight sites are nonlinear and exhibit different degrees of steepness. ESO efficiency is higher for NREL 5 MW turbines, with flatter Pareto fronts across all sites, whereas IEA 15 MW turbines show steeper Pareto fronts. This means that with relatively small AEP loss, it would be possible to extend the NREL 5 MW turbine end of incubation considerably.

The second metric is how much AEP loss is needed to achieve a specific number of years to the end of incubation. The atlas at 5, 10, 15, and 20 years for each of the three turbines is provided. NREL 5 MW would reach 20 years at the end of incubation without applying ESO except in parts of the Atlantic Ocean, the Norwegian Sea, and the North Sea. DTU 10 MW would reach 20 years at the end of incubation in most onshore places, except in primarily exposed western coastal areas, but would need ESO in most offshore areas. IEA 15 MW would reach 20 years only in limited onshore areas, such as parts of the Alps, Norway, Sweden, and Finland. However, because these areas have a high number of low-quality IMERG data, the results are less trustworthy than in other parts of Europe.

The probabilistic Monte Carlo simulations conducted for the eight sites show uncertainty in the end of incubation and ESO efficiency. There is variability in the expected end of incubation under normal conditions (i.e., without curtailment). The uncertainty is higher at some sites than at others due to differences in the distributions of concurrent rainfall and wind speed among sites. Moray East shows less variability than Rézentières. The application of ESO at selected AEP loss levels (0.2% and 0.4%) shows that uncertainty increases with larger AEP loss. Interestingly, the increase in uncertainty is highly nonlinear. The difference between the minimum and maximum end of incubation between 0 and 0.4% AEP loss roughly doubles for Moray East, Båtskär, Buseco, Levenmouth and Risø, triples for Alaiz and Rézentières, and quadruples for San Gregorio.

The IMERG and NEWA datasets have 30-minute temporal resolution. The resolution is sufficient to assess the end of incubation in normal operation (without curtailment). Thus, the relevance of ESO can be assessed in the current analysis, i.e., whether it is relevant to consider a repair strategy or an ESO strategy for turbines operating at the location. A limitation of the

https://doi.org/10.5194/wes-2026-225
Preprint. Discussion started: 25 November 2026
© Author(s) 2026. CC BY 4.0 License.



ESO efficiency atlas prevails. The 30-minute temporal resolution is not sufficient to assess ESO efficiency in detail. The potential impact of implementing an ESO control strategy cannot be fully resolved. Campobasso et al. (2026) investigated ESO efficiency at different temporal resolutions and found that ESO effectiveness increases with higher frequency, especially for sites with rapid variations in rainfall rate. The most intensive and damaging rain events are often very short-lived. Short-lived rain events are frequent, and a 30-minute curtailment is far too long. The minute scale is appropriate for increasing ESO efficiency (Tilg et al., 2020; Pryor et al., 2025).

It must be assumed that the ESO efficiency presented in the atlas and at the eight sites severely underestimates the true value. Hasager et al. (in review) quantified the difference in ESO efficiency between IMERG and NEWA, and between high-temporal-resolution disdrometer and sonic wind-speed data, at the Risø site. The study showed that high-frequency data used to assess ESO efficiency yielded flatter Pareto fronts than IMERG and NEWA data (Hasager et al., in review). Reducing the high-frequency data to 30-minute intervals yields a Pareto front that is nearly as steep as those of IMERG and NEWA. The original high-frequency ESO Pareto front for a given AEP loss roughly doubles the period to the end of incubation compared to the 30-minute data. The logic of more efficient ESO using high-frequency data relies on short-lived, minute-scale rain events occurring, and a control strategy curtailing at 30-minute intervals would inevitably include dry conditions. A future investigation could test ESO efficiency Pareto fronts at locations with accessible high-frequency data to examine how different weather conditions affect ESO efficiency compared to 30-minute data.

The modelling presented herein is based on a clean power curve, i.e., no change in the power curve due to erosion, which, however, is not an accurate representation of eroded blades (Maniaci et al., 2025; Forsting et al., 2026; Olsen et al., 2026). The modelling could be refined using a moderate- and severe-leading-edge-erosion state of the power curve (Visbech et al., 2024; Campobasso et al., 2023, 2026). The addition of the eroded power curve to the analysis would be expected to increase the efficiency of ESO.

Field-based assessments would be relevant in future studies, complementing results from laboratory studies (Sánchez et al., 2026). In our study, the material response (VH-curve) is assessed deterministically, and including material uncertainties would increase the total uncertainty at the end of incubation and in ESO efficiency (Visbech et al., 2025; Hasager et al., in review). Solid precipitation has been excluded from the current study. Analysis from the US suggests that ESO could be effective against hail (Pryor and Barthelmie, 2026). This should be investigated in Europe in the future.

6. Conclusion

In this study, the first erosion risk atlas for Europe was developed. The study is based on rainfall from IMERG, a global, half-hourly satellite-based product, and wind speeds from the NEWA model, covering 9 years from 2014 to 2022. An impingement damage model derived from comprehensive rain erosion test data from commercial coating is selected, and end-of-incubation results for three reference turbines, NREL 5 MW, DTU 10 MW and IEA 15 MW, are presented. To increase computational

https://doi.org/10.5194/wes-2026-225
Preprint. Discussion started: 25 November 2026
© Author(s) 2026. CC BY 4.0 License.



speed in producing the atlas, an empirical method that represents the distributions of concurrent rainfall and wind speed data is applied. The method closely reflects a time-series method applied at selected sites in contrasting climates. The atlas includes three main layers:

- Spearman correlation map between rainfall and wind speed showing positive values in most places, particularly offshore, indicating that rainfall is more likely to occur in windy than in calm conditions. At high-dependency sites, erosion risk is higher than at low-dependency sites, even at the same average rainfall and wind speed.
- End-of-incubation maps show large variation between turbines, with larger turbines eroding faster than smaller ones due to differences in hub height, minimum rpm, rated speed, and tip speed. The end of incubation varies geographically, generally with faster erosion offshore in the Atlantic, Norwegian, and North Seas, and slower erosion inland.
- Erosion-safe operation (ESO) efficiency maps representing the extended incubation end at 0.2% and 0.4% AEP loss are produced. Additionally, ESO efficiency maps reversing the metric, showing the AEP loss needed to achieve 5-, 10-, 15-, and 20-year end of incubation, are presented. Large variability between turbines and across geographic regions is noted.

Limitations of the study relate to the quality of input data. IMERG shows a high fraction of low-quality data in the Alps, parts of Norway, Sweden, and Finland. NEWA-modeled winds are better resolved in flatter terrain than in mountainous terrain. The atlas is likely less accurate in these regions than elsewhere in Europe. Other limitations of IMERG are that hail cannot be separated but is collectively referred to as probability of solid precipitation; there may be mismatch between observed rain from rain gauge and IMERG; and IMERG areal-average rain intensity versus local point observed rain intensity may vary. Mismatch between observed rain and modelled winds through the combination of IMERG and NEWA could prevail.

The atlas is based on 9 years of data. A longer time series would enable more reliable end-of-incubation values, as large interannual variation prevails. Decadal changes in rain and wind climates are likely to occur in response to climate change.

Probabilistic Monte Carlo simulations across eight sites with contrasting climates show that weather conditions drive differences in the uncertainty of the end of incubation and in ESO efficiency.

The atlas is based on a 30-minute temporal resolution. To assess the end of incubation, this is considered sufficient, while ESO efficiency values would be conservative. Using higher-frequency, minute-scale data would better resolve atmospheric conditions for short-lived rain events, potentially improving ESO efficiency.

Code and data availability

Vinod, A., Toft, L. D. D. S., Dimitriadou, K., Hasager, C. B. 2026. Atlas data set on leading-edge erosion risk in Europe based on IMERG. 10.5281/zenodo.21062880 (accessed 18 November 2026)

The code of Madsen, J.V. is available at https://zenodo.org/records/17414783. (accessed 18 November 2026)

NEWA data are accessible from www.neweuropeanwindatlas.eu. (accessed 18 November 2026)

IMERG data are accessible from https://disc.gsfc.nasa.gov/. (accessed 18 November 2026)

https://doi.org/10.5194/wes-2026-225
Preprint. Discussion started: 25 November 2026
© Author(s) 2026. CC BY 4.0 License.



eawe european academy of wind energy
Open Access WIND ENERGY SCIENCE DISCUSSIONS

Author contributions

Author contributions. CBH writing — original draft, Methodology, Funding acquisition, Conceptualization. AV writing—review and editing, Methodology, Data analysis, Visualization, Figs. 3-4, 7, 9-11. LDDST writing — review and editing, Visualization, Figs. 1-2, 5-6, 8. KD writing—review and editing.

Competing interests

The authors declare no conflict of interest.

Disclaimer

Copernicus Publications remains neutral with regard to jurisdictional claims made in the text, published maps, institutional affiliations, or any other geographical representation in this paper. While Copernicus Publications makes every effort to include appropriate place names, the final responsibility lies with the authors. Views expressed in the text are those of the authors and do not necessarily reflect the views of the publisher.

Acknowledgements

We acknowledge the Goddard Earth Sciences Data and Information Services Center (GES DISC) for the GPM IMERG Final Precipitation product (Huffman et al., 2020) and wind speed data from NEWA. We thank the NEWA team for their support in extracting wind speed data. We gratefully acknowledge the computational and data resources provided on the Sophia HPC Cluster at the Technical University of Denmark, DOI: 10.57940/FAFC-6M81. We thank Jens Visbech Madsen for developing the code.

Financial support

This work is supported by the AIRE project, which has received funding from the European Union under the grant agreement 101083716.

https://doi.org/10.5194/wes-2026-225
Preprint. Discussion started: 25 November 2026
© Author(s) 2026. CC BY 4.0 License.



References

Badger, M., Zuo, H., Hannesdóttir, Á., Owda, A., Hasager, C.: Lifetime prediction of turbine blades using global precipitation products from satellites, Wind Energ. Sci, 7, 2497–2512, https://doi.org/10.5194/wes-7-2497-2022, 2022.

Bak, C., Zahle, F., Bitsche, R., Kim, T., Yde, A., Henriksen, L. C., Andersen, P. B., Natarajan, A., Hansen, M. H.: Description of the DTU 10 MW Reference Wind Turbine. DTU Wind Energy Report-I-0092, Roskilde, Denmark, https://www.hawc2.dk/models/dtu-10-mw, 2013.

Barfknecht, N., von Terzi, D.: Aerodynamic interaction of rain and wind turbine blades: the significance of droplet slowdown and deformation for leading-edge erosion, Wind Energ. Sci., 9, 2333–2357, https://doi.org/10.5194/wes-9-2333-2024, 2024.

Bech, J. I., Hasager, C. B., Bak, C.: Extending the life of wind turbine blade leading edges by reducing the tip speed during extreme precipitation events, Wind Energy Sci., 3(2), 729-748, https://doi.org/10.5194/wes-3-729-2018, 2018.

Bech, J. I., Johansen, N. F., Madsen, M. B., Hannesdóttir, Á., Hasager, C. B.: Experimental study on the effect of drop size in rain erosion test and on lifetime prediction of wind turbine blades, Renew. Energy, 197, 776–789, https://doi.org/10.1016/j.renene.2022.06.127, 2022.

Best, A.: The size distribution of raindrops, Q. J. R. Meteorol. Soc., 76, 16–36, https://doi.org/10.1002/qj.49707632704, 1950.

Caboni, M., van Dalum, G.: Developing an atlas of rain-induced leading edge erosion for wind turbine blades in the Dutch North Sea, Wind Energ. Sci., 10, 1887–1906, https://doi.org/10.5194/wes-10-1887-2025, 2025.

Caboni, M., Slot, H. M., Bergman, G., Wouters, D. A. J., Meijer, H. J. V. D. M.: Evaluation of wind turbine blades' rain-induced leading edge erosion using rainfall measurements at offshore, coastal and onshore locations in the Netherlands, Journal of Physics, 2767, https://doi.org/10.1088/1742-6596/2767/6/062003, 2024.

Campobasso, M. S., Castorrini, A., Ortolani, A., Minisci, E.: Probabilistic analysis of wind turbine performance degradation due to blade erosion accounting for uncertainty of damage geometry, Renew. Sustain. Energy Rev., 178, 113254, https://doi.org/10.1016/j.rser.2023.113254, 2023.

Campobasso, M. S., Rose, M. S., Shende, S., Adirosi, E., Pace, G., Silvestri, L. D., Dimitriadou, K., Vinod, A., Hasager, C. B., Sánchez, F., Castorrini, A.: Development, performance and energy trade-off analyses of wind turbine precipitation-reactive control at offshore and onshore sites in Western Europe, Renew. Energy, 262, 125357, https://doi.org/10.1016/j.renene.2026.125357, 2026.

Castorrini, A., Barnabei, V. F., Domenech, L., Šakalyté, A., Sánchez, F., Campobasso, M. S.: Impact of meteorological data factors and material characterization method on the predictions of leading edge erosion of wind turbine blades, Renew. Energy, 227, 120549, https://doi.org/10.1016/j.renene.2024.120549, 2024.

Cornes, R. C., van den Schrier, G., van den Besselaar, E. J. M., Jones, P. D.: An ensemble version of the E-OBS temperature and precipitation data sets, J. Geophys. Res. Atmos.,123, 9391–9409, https://doi.org/10.1029/2017JD028200, 2018.

https://doi.org/10.5194/wes-2026-225
Preprint. Discussion started: 25 November 2026
© Author(s) 2026. CC BY 4.0 License.

Dimitriadou, K., Hasager, C. B.: Comparison of GPM IMERG V07B versus IMERG V06B Precipitation in Northern Spain and their application for wind turbine blade lifetime estimation, Science of Remote Sensing, 14, 100458, https://doi.org/10.1016/j.srs.2026.100458, 2026.

Dimitriadou, K., Hasager, C. B., Nouqueret, E. C., Hannesdóttir, Á.: Quality assessment of the GPM IMERG product for lifetime prediction of turbine blades in complex terrain, J. Phys.: Conf. Ser., 2767, 042010, https://doi.org/10.1088/1742-6596/2767/4/042010, 2024.

DNV: DNV-RP-0573 Evaluation of Erosion and Delamination for Leading Edge Protection Systems of Rotor Blades, Det Norske Veritas: Høvik, Norway, 2021.

Dörenkämper, M., Olsen, B. T., Witha, B., Hahmann, A. N., Davis, N. N., Barcons, J., Ezber, Y., García-Bustamante, E., González-Rouco, J. F., Navarro, J., Sastre-Marugán, M., Sīle, T., Trei, W., Žagar, M., Badger, J., Gottschall, J., Sanz Rodrigo, J., and Mann, J.: The Making of the New European Wind Atlas – Part 2: Production and evaluation, Geosci. Model Dev., 13, 5079–5102, https://doi.org/10.5194/gmd-13-5079-2020, 2020.

Forsting, A. M., Dicholkar, A., Sørensen, N. N., Olsen, A. S., Bak, C., Theron, J. N., Aihara, A., Caboni, M., Ravishankara, A. K., Vimalakanthan, K., Bretos, D., Mendez, B., Campaña-Alonso, G., Jimenez, O. P., Grasso, F., Campobasso, M. S., Maniaci, D.: Benchmarking aerodynamic codes for 2D aerofoils with leading edge erosion, IOP Publishing, 042037, https://doi.org/10.1088/1742-6596/3224/4/042037, 2026.

Gaertner, E., Rinker, J., Sethuraman, L., Zahle, F., Anderson, B., Barter, G., Abbas, N., Meng, F., Bortolotti, P., Skrzypinski, W., et al.: Definition of the IEA Wind 15-Megawatt Offshore Reference Wind Turbine, IEA Wind TCP Task 37 Technical Report, National Renewable Energy Laboratory (NREL): Golden, CO, USA, http://dx.doi.org/10.2172/1603478, 2020.

Ghasemifard, H.; Groenemeijer, P.; Battaglioli, F.; Púčik, T.: Do changing circulation types raise the frequency of summertime thunderstorms and large hail in Europe? Environ. Res.: Climate, 3, 015008, https://iopscience.iop.org/article/10.1088/2752-5295/ad22ec, 2024

Haakenstad, H., Breivik, Ø., Furevik, B. R., Reistad, M., Bohlinger, P., Aarnes, P. O. J.: NORA3: A Nonhydrostatic High-Resolution Hindcast of the North Sea, the Norwegian Sea, and the Barents Sea, J. Appl. Meteorol. Climatol., 60, 1443–1464, https://doi.org/10.1175/JAMC-D-21-0029.1, 2021.

Hannesdóttir, Á., Kral, S.T., Reuder, J., Hasager, C. B.: Rain erosion atlas for wind turbine blades based on ERA5 and NORA3 for Scandinavia, Results Eng., 22, 102010, https://doi.org/10.1016/j.rineng.2024.102010, 2024a.

Hasager, C., Vejen, F., Bech, J., Skrzypiński, W., Tilg, A.-M., Nielsen, M.: Assessment of the rain and wind climate with focus on wind turbine blade leading edge erosion rate and expected lifetime in Danish Seas, Renew. Energy, 149, 91–102, https://doi.org/10.1016/j.renene.2019.12.043, 2020.

Hasager, C. B., Vejen, F., Skrzypiński, W. R., Tilg, A.-M.: Rain Erosion Load and Its Effect on Leading-Edge Lifetime and Potential of Erosion-Safe Mode at Wind Turbines in the North Sea and Baltic Sea, Energies, 14(7), 1959, https://doi.org/10.3390/en14071959, 2021.

https://doi.org/10.5194/wes-2026-225
Preprint. Discussion started: 25 November 2026
© Author(s) 2026. CC BY 4.0 License.

Hasager, C. B., Vinod, A., Toft, L. D. D. S., and Dimitriadou, K.: Leading-edge erosion risk: Assessment of uncertainties, Wind Energ. Sci. Discuss. [preprint], https://doi.org/10.5194/wes-2026-136, in review, 2026.

Hersbach, H., Bell, B., Berrisford, P., Hirahara, S., Horányi, A., Muñoz-Sabater, J., Nicolas, J., Peubey, C., Radu, R., Schepers, D., et al.: The ERA5 global reanalysis, Q. J. R. Meteorol. Soc., 146, 1999–2049, https://doi.org/10.1002/qj.3803, 2020.

Huffman, G.J., Bolvin, D. T., Nelkin, E. J., Wolff, D. B., Adler, R. F., Gu, G., Hong, Y., Bowman, K. P., Stocker, E. F.: Integrated Multi-satellite Retrievals for the Global Precipitation Measurement (GPM) Mission (IMERG), In Satellite Precipitation Measurement; Levizzani, V., Kidd, C., Kirschbaum, D. B., Kummerow, C. D., Nakamura, K., Turk, F. J., Eds., Springer: Cham, 67, pp. 343–353. https://doi.org/10.1007/978-3-030-24568-9_19, 2020.

Huffman, G. J., Bolvin, D. T., Joyce, R., Kelley, O. A., Nelkin, E. J., Tan, J., Watters, D. C., West, B. J.: Integrated Multi-satellitE Retrievals for GPM (IMERG) Technical Documentation, Technical Report, NASA Goddard Space Flight Center, https://disc.gsfc.nasa.gov/datasets/GPM_3IMERGHH_07/summary?keywords=imerg, 2023.

IPCC, Intergovernmental Panel on Climate Change (IPCC). Weather and Climate Extreme Events in a Changing Climate. Chapter 11. In: Climate Change 2021 – The Physical Science Basis: Working Group I Contribution to the Sixth Assessment Report of the Intergovernmental Panel on Climate Change, Cambridge University Press, 1513-1766, 2023.

Ivanova, T.: High-impact wind and precipitation conditions for offshore wind farms from numerical weather prediction and remote sensing. PhD Thesis, Vrije Universiteit Brussel, The von Karman Institute for Fluid Dynamics, 2025.

Ivanova, T., Palatos-Plexidas, A., Porchetta, S. Buckingham, S., van Beeck, J., De Cruz, L., Helsen, J., Munters, W.: Precipitation Conditions in Offshore Wind Farm Zones: Insights from Satellites and Weather Simulations. J. Phys.: Conf. Ser. 3131 012005DOI 10.1088/1742-6596/3131/1/012005, 2025.

Jonkman, J., Butterfield, S., Musial, W., Scott, G.: Definition of A 5-MW Reference Wind Turbine for Offshore System Development, Technical Report NREL/TP-500-38060, National Renewable Energy Laboratory (NREL): Golden, CO, USA, http://dx.doi.org/10.2172/947422, 2009.

Keegan, M. H, Nash, D. H., Stack, M.M.: On erosion issues associated with the leading edge of wind turbine blades, J. Phys. D: Appl. Phys. 46, https://doi.org/10.1088/0022-3727/46/38/383001, 2013.

Madsen, J. V., Hannesdóttir, Á., Vinod, A., Hasager, C. B.: D4.5- Erosion-safe operation design tool: Dedicated Toolbox Design, AIRE, 2026.

Maniaci, D., Forsting, A. M., Barlas, A., Bak, C., Olsen, A. S.: Model to predict annual energy production loss based on blade erosion class, Technical report, IEA Task 46, https://doi.org/10.2172/2530796, 2025.

Mishnaevsky Jr., L., Hasager, C. B., Bak, C., Tilg, A.-M., Bech, J. I., Doagou Rad, S., Fæster, S.: Leading edge erosion of wind turbine blades: Understanding, prevention and protection, Renewable Energy, 169, 953-969, https://doi.org/10.1016/j.renene.2021.01.044, 2021.

https://doi.org/10.5194/wes-2026-225
Preprint. Discussion started: 25 November 2026
© Author(s) 2026. CC BY 4.0 License.

Nash, J.W.K.; Zekos, I.; Stack, M.M.: Mapping of Meteorological Observations over the Island of Ireland to Enhance the Understanding and Prediction of Rain Erosion in Wind Turbine Blades. Energies, 14, 4555, https://doi.org/10.3390/en14154555, 2021.

NEWA: New European Wind Atlas, DTU, Roskilde, Denmark, https://www.neweuropeanwindatlas.eu/, 2026.

Olsen, A. S., Forsting, A. M., Fischer, A., Lylloff, O., Sørensen, N. N., Dicholkar, A. C., Madsen, J., Munoz, A., Vronsky, T., Grasso, F., Gaudern, N., Akay, B., Kommer, R., & Bak, C.: A categorisation scheme for energy losses and noise increase due to leading edge roughness. In WindEurope Annual Event 2026 IOP Publishing. https://doi.org/10.1088/1742-6596/3232/1/012012, 2026.

Punge, H. J., Kunz, M.: Hail observations and hailstorm characteristics in Europe: A review, Atmospheric Research, 176–177,159-184. https://doi.org/10.1016/j.atmosres.2016.02.012, 2016.

Pryor, S. C., Barthelmie, R. J.: Hail as a damage vector for renewable energy, IScience, 29, https://doi.org/10.1016/j.isci.2025.114439, 2026.

Pryor, S. C., Coburn, J. J., Barthelmie, R. J.: Spatiotemporal Variability in Wind Turbine Blade Leading Edge Erosion, Energies, 18(2), 425, https://doi.org/10.3390/en18020425, 2025.

Retalis A., Katsanos, D., Michaelides, S., Tymvios, F.: Evaluation of high-resolution satellite precipitation data over the Mediterranean Region. Chapter 5 in Precipitation Science. Editor: Silas Michaelides, Elsevier, p. 159-175, 10.1016/B978-0-12-822973-6.00017-2, 2022.

Sakai, E., Hashimoto, A., Nanko, K., Takahashi, T., Nishida, H., Tamura, H., Hattori, Y., Kitano, Y.: Rain Erosion Atlas of Wind Turbine Blades for Japan Based on Long-Term Meteorological and Climate Dataset CRIEPI-RCM-Era2, Wind, 6, 7, https://doi.org/10.3390/wind6010007, 2026.

Sánchez, F., Hao, H., Domenech, L., Hardalupas, Y., Dyer, K., García-Peñas, V., Charalambides, M., Ibáñez-Arnal, M., Sergis, A., Taylor, A. M. K. P.: Rain erosion damage initiation assessment of wind turbine blades leading edge protection systems based on laboratory testing data: a review and case study, Results in Engineering, 30, 110327, https://doi.org/10.1016/j.rineng.2026.110327, 2026.

Simon, J. E., Bajpai, A., Johansen, N. F.-J., Hannesdóttir, Á., Hasager, C.: Lifetime estimation of blade erosion using rain erosion test data with different analysis methods, Wind Energy 29, no. 11: e70140, https://doi.org/10.1002/we.70140, 2026

Skamarock, W. C., Klemp, J. B., Dudhia, J., Gill, D. O., Liu, Z., Berner, J., ... & Huang, X. Y.: A description of the advanced research WRF version 4. NCAR tech. note, https://csdms.colorado.edu/wiki/Reference:Reference-004125, 2019.

Solbrekke, I.M., Sorteberg, A., Haakenstad, H.: The 3 km Norwegian reanalysis (NORA3) – a validation of offshore wind resources in the North Sea and the Norwegian Sea, Wind Energy Sci., 6, 1501–1519, https://doi.org/10.5194/wes-6-1501-2021, 2021.

Taszarek, M.; Allen, J. T.; Groenemeijer, P.; Edwards, R.; Brooks, H.E.; Chmielewski, V. Enno, S.: Severe Convective Storms across Europe and the United States. Part I: Climatology of Lightning, Large Hail, Severe Wind, and Tornadoes. J. Climate, 33, 10239–10261, https://doi.org/10.1175/JCLI-D-20-0345.1, 2020.

https://doi.org/10.5194/wes-2026-225
Preprint. Discussion started: 25 November 2026
© Author(s) 2026. CC BY 4.0 License.

Tilg, A.-M., Hasager, C. B., Kirtzel, H.-J., Hummelshøj, P.: Brief communication: Nowcasting of precipitation for leading-edge-erosion-safe mode, Wind Energ. Sci. 5, 977–981, https://doi.org/10.5194/wes-5-977-2020, 2020.

Varga, Á.J.; Breuer, H.: Evaluation of multiple surface-, satellite-, reanalysis-, and WRF model-based gridded precipitation datasets over south-east Central Europe, Atmospheric Research, 298, https://doi.org/10.1016/j.atmosres.2023.107138, 2024.

Verma, A. S., Jiang, Z., Ren, Z., Caboni, M., Verhoef, H., Mijle Meijer, H. v. d., Castro, S. G. P., Teuwen, J. J. E.: A probabilistic long-term framework for site-specific erosion analysis of wind turbine blades: A case study of 31 Dutch sites, Wind Energy, 24,1314–1336, https://doi.org/10.1002/we.2634, 2021.

Vinod, A., Toft, L. D. D. S., Dimitriadou, K., Hasager, C. B. 2026. Atlas data set on leading-edge erosion risk in Europe based on IMERG. 10.5281/zenodo.21062880

Visbech, J., Göçmen, T., Hasager, C. B., Shkalov, H., Handberg, M., Nielsen, K. P.: Introducing a data-driven approach to predict site-specific leading-edge erosion from mesoscale weather simulations, Wind. Energy Sci., 8,173–191, http://dx.doi.org/10.5194/wes-8-173-2023, 2023.

Visbech, J., Göçmen, T., Özçakmak, Ö. S., Forsting, A. M., Hannesdóttir, Á., Réthoré, P. -E.: Aerodynamic effects of leading-edge erosion in wind farm flow modeling, Wind Energy Sci., 9, 1811-1826, https://doi.org/10.5194/wes-9-1811-2024, 2024.

Visbech, J., Hasager, C. B., Göçmen, T., Réthoré, P. - E.: Copula-based joint distributions of rain and wind for leading edge erosion risk atlas, Renew. Energy, 253,123358, https://doi.org/10.1016/j.renene.2025.123358, 2025.

Xiong, W., Tang, G., Wang, T., Ma, Z., Wan, W.: Evaluation of IMERG and ERA5 Precipitation-Phase Partitioning on the Global Scale, Water, 14, 1122, https://doi.org/10.3390/w14071122, 2022.